S1. CqsS membrane topology prediction

CqsS is predicted to have four or six transmembrane helices depending on the prediction algorithm chosen. Here, we use the program Topred (1) with two different hydrophobicity scales to illustrate the differences. Using Topred with the KD-scale, CqsS is predicted to have six transmembrane helices consisting of residues 17-37, 47-67, 78-98, 101-121, 124-144, and 154-172. Using the same program with the GES-scale, CqsS is predicted to have four transmembrane helices consisting of residues 17-37, 78-98, 124-144, and 154-174. Out of forty active CqsS-LacZ fusions, using the four helix model, eight clones would have fusions in the periplasm (residues 48, 57, 58, 62, 68, 73). By contrast, no active CqsS-LacZ clones would be linked to periplasmic residues according to the 6-helix model. Likewise, out of forty active CqsS-PhoA fusions, four clones are predicted to have fusions in the cytoplasm according to the 4-helix model (residues 99, 100, 102, 107). By contrast, no active CqsS-PhoA clones are predictied to be cytoplasmic according to the 6-helix model. Thus, we conclude that the 6-helix model is consistent with the correct CqsS transmembrane topology.

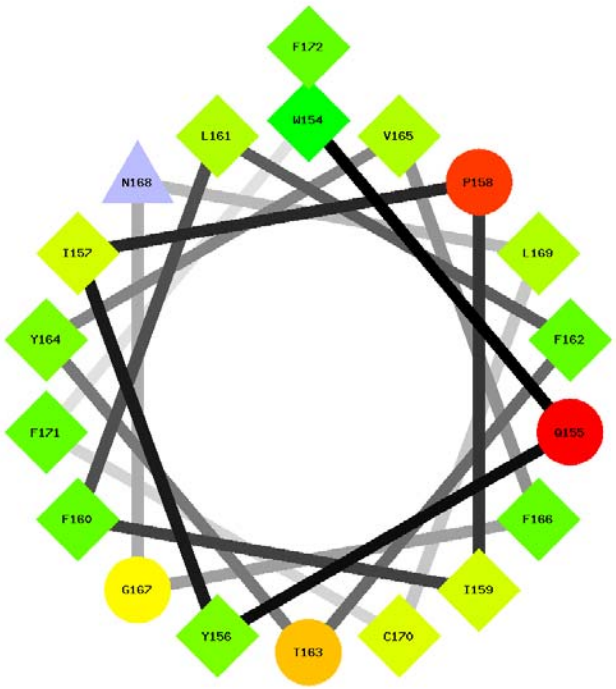

The helical wheel projection of the sixth transmembrane helix is drawn using a program available at http://trimer.tamu.edu/cgi-bin/wheel/wheel.pl. The figure shows that F162, F166, and C170 are predicted to lie on the same surface, while F160 is predicted to lie on the opposite face.

1. von Heijne G (1992) Membrane protein structure prediction. Hydrophobicity analysis and the positive-inside rule. *J Mol Biol* 225:487-494.

S2. CqsS sequence alignment and CqsS mutant phenotypes

CqsS alignments are shown for *cqsS* genes that are linked to putative *cqsA* genes in their respective chromosomes. The transmembrane regions were predicted and aligned with TMHMM and ClustalW, respectively. Seventeen residues are 100% conserved among these CqsS homologs as shown below (denoted by * under the alignment):

```
Chlorobium_ferrooxidans_DSM_13      -------MHILKNKAREIIEHAEPNLGVVGLFGFLGYPVYYLIWTYIFPQ 43
Chlorobium_phaeobacteroides_DS      -------MQKLKSLSKRIIEHAEPNLGIIGIFTTLGYPVYYIIWTFLFPQ 43
Chlorobium_limicola_DSM_245         -------MQRLKQKAINIVEHAEPNLPIIGLFATVGYPLFYIVWKYLFPQ 43
Vibrio_angustum_S14                 --------MSIKNRINNVYRYFEPNLIIIGYLGSIGFPLYFFVWHYLFPQ 42
Photobacterium_sp._SKA34            --------MSIKNRINNVYRYFEPNLIIIGYLGSIGFPLYFFVWHYLFPQ 42
Vcholerea_C6706str                  -------MIVSMDVIKRVYQYAEPNLSLVGWMGMLGFPAYYFIWEYWFPQ 43
Vcholerae_1587                      -------MIVSMDVIKRVYQYAEPNLSLVGWMGMLGFPAYYFIWEYWFPQ 43
Vcholerae_V51                       -------------------------------MGMLGFPAYYFIWEYWFPQ 19
Vibrio_shilonii_AK1                 -------------------------------MGILGFPLYYVIWKYVFPQ 19
Vibrio_sp_MED222                    -----------MNAIRKVYQYAEPNLTLVGWMGFVGFPAYYIVWEFLFPQ 39
Vibrio_splendidus_12B01             -----------MNAIRKVYQYAEPNLTLVGWMGFVGFPIYYIVWEFLFPQ 39
Vibrionales_bacterium_SWAT-3        -----------MNAIRKVYQYAEPNLTLVGWMGFVGFPVYFVVWEYLFPQ 39
Vibrio_harveyi_ATCC_BAA-1116        -----------MDAIRKVYQYAEPNLSLVGWMGFIGFPIYYIVWEFMFPQ 39
Vibrio_harveyi_HY01                 -------------------------------MGFVGFPIYYIVWEFMFPQ 19
Vibrio_campbellii_AND4              -----------MDAIRKVYQYAEPNLTLVGWMGFVGFPIYYIVWAFMFPQ 39
Valginolyticus_12G01                -----------MDSIRKVYQYAEPNLTLVGWMGFLGFPLYYFVWEFAFPQ 39
Vibrio_sp_Ex25                      -----------MDSIRKVYQYAEPNLTLVGWMGFLGFPLYYFVWDFVFPQ 39
Vibrio_parahaemolyticus_RIMD_2      -----------MDSIRKVYEYAEPNLTLVGWMGFIGFPLYYFVWDFMFPQ 39
Vibrio_parahaemolyticus_AQ3810      -------------------------------MGFIGFPLYYFVWDFMFPQ 19
Photobacterium_profundum_SS9        --------MSVKTAIQKVYQYAEPNLSLVGWMGFIGFPFYYVIWAYIFPQ 42
Photobacterium_profundum_3TCK       --------MSVKTAMQKVYQYAEPNLSLVGWMGFIGFPLYYIVWAYIFPQ 42
Legionella_pneumophila_str_Cor      MSQLKRIVKHLDESMQRSLSNSAHQLVAVGAIAFVGFPLFYVIWAFWLPQ 50
                                                          :  :*:* ::.:* : :**

Chlorobium_ferrooxidans_DSM_13      PYENLPLRIFCAFISIPWVLYRFIPKKLKEIFPVYFFISLFIVIPFFFSF 93
Chlorobium_phaeobacteroides_DS      PYENLMLRIFCAFISIPCILYRHIPVSLKKFFPFYFYLTFFIDVPYFFSF 93
Chlorobium_limicola_DSM_245         HYENLTLRLIEAVISLPWLFYRYLPKKAKTIFPVYFFISVPVLLPFFFHF 93
Vibrio_angustum_S14                 PYENFLLRLFCGTLFIPFILKDHLPYWFLRYKAIHFIATITIGLPFFFSY 92
Photobacterium_sp._SKA34            PYENFLLRLFCGSLFIPFVLKDHLPYWFLRYKAIHFIATITIGLPFFFSY 92
Vcholerea_C6706str                  SYENLGLRCAAAVLFGGLVFRDSMPKKWQRYMPGYFLFTIGFCLPFFFAF 93
Vcholerae_1587                      SYENLGLRCAAAVLFGGLVFRDSMPKKWQRYMPGYFLFTIGFCLPFFFAF 93
Vcholerae_V51                       SYENLGLRCAAAVLFGGLVFRDSMPKKWQRYMPGYFLFTIGFCLPFFFAF 69
Vibrio_shilonii_AK1                 PYESELLRTIGAIMLIGFILLRAFSEKTKRILPYYYLVVIGFTLPFFFCY 69
Vibrio_sp_MED222                    PYENLAVRLFCSVLFLGIVVRNRIPFDWRKYLPAYYQVAITLCLPCFFFY 89
Vibrio_splendidus_12B01             PYENLMLRLFCSVLFFGIIYRNRVPFEWRKYLPAYYQVAVTICLPGFFFY 89
Vibrionales_bacterium_SWAT-3        PYENLTLRLLCSVLFFGIIFRKHVPFEWRKYLPAYYQVAITLCLPCFFFY 89
Vibrio_harveyi_ATCC_BAA-1116        PYENLPLRILCSVLFFGIIYRNRTPFEWRGFLPAYYQVVTTLCLPCFFFY 89
Vibrio_harveyi_HY01                 PYENLPLRILCSVLFFGIIYRNRAPFEWRRFLPAYYQVVTTLCLPCFFFY 69
Vibrio_campbellii_AND4              PYESLPFRILCSILFFGIICRNHMPFKWRKFLPAYYQLVTTLCLPCFFFY 89
Valginolyticus_12G01                AYENLSLRLFCSLLFFGIIFRNRLSSTWRDYVPIYYQVTITLCLPFFFFY 89
Vibrio_sp_Ex25                      AYENLPLRLFCSLLFFGIIFRNRLSSTWRKYIHIYYQVTITICLPFFFFY 89
Vibrio_parahaemolyticus_RIMD_2      SYENLPLRLFCSALFFGIIFRNRLSSSWRKYVHVYYQITITTCLPFFFFY 89
Vibrio_parahaemolyticus_AQ3810      SYENLPLRLFCSALFFGIIFRNRLSSSWRKYVHVYYQITITTCLPFFFFY 69
Photobacterium_profundum_SS9        PYENLTLRLACSLLFLGLIVRKKLKRKWRNRMHLYYQMVITLCLPFFFFY 92
Photobacterium_profundum_3TCK       PYENLTLRLACSLLFLGIVVRKKLKRQWRNRMHLYYQLVITLCLPFFFFY 92
Legionella_pneumophila_str_Cor      PYENLPLRLIGSFLGLGLMLTPYWPLKWKQYLSWYWFLTLLFTLPYFFTF 100
                                     **.  .*   . :    :               ::       :* ** :
```

```
Chlorobium_ferrooxidans_DSM_13      MTLKNEFSVVWAMSTMAGLFLLTLLMSDRVLVSIMTGAGFMAAYVTVLTI 143
Chlorobium_phaeobacteroides_DS      MLLKNECSTVWTMSLLTGIFMLILILSNWMVVSIMTILGFITAYATVMFL 143
Chlorobium_limicola_DSM_245         MMLRNEWSIAWAMSSMACLFMLILIVYDWIFICIITLSGFVLAYAAVYAL 143
Vibrio_angustum_S14                 MLIMNDWSIPWIMSFMAALFLSILLIYDAYIISAISIIGITLGALFSYGF 142
Photobacterium_sp._SKA34            MLIMNHWSIPWVMSFMAALFLSILLIYDAYIISVISIIGISLGALFSYGF 142
Vcholerea_C6706str                  MMLMNDWSTIWAMSFMASIFLHILLVHDTRVMALQALFSVLVAYLAVYGL 143
Vcholerae_1587                      MMLMNDWSTIWAMSFMASIFLHILLVHDTRVMALQALFSVLVAYLAVYGL 143
Vcholerae_V51                       MMLMNDWSTIWAMSFMASIFLHILLVHDTRVMALQALFSVLVAYLAVYGL 119
Vibrio_shilonii_AK1                 MMLMNNWTTVWVMSFMSSIFLHILFIYDTRIMVAQAVISVVSAVILAYIM 119
Vibrio_sp_MED222                    MLLMNNWSNVWVMSFMSAIFLHILLVHVTRVMFAQTFAGIGIATLCAWVA 139
Vibrio_splendidus_12B01             MLLMNNWSNVWVMSFMSAIFLHILLVHVTRVMFAQTFAGIGMATLCAWIA 139
Vibrionales_bacterium_SWAT-3        MLLMNNWSNVWVMSFMSAIFLHILLVHVTGVMFAQTFAGIGIATFCAWVA 139
Vibrio_harveyi_ATCC_BAA-1116        MLLMNNWSNVWVMSFMSAIFLHILLVHITSVMFVQTFVGIGLATFFAWVA 139
Vibrio_harveyi_HY01                 MLLMNNWSNVWVMSFMSAIFLHILLVHITSVMFAQTFAGIGLATFFAWVA 119
Vibrio_campbellii_AND4              MLLMNNWSNVWVMSFMSAIFLHILLVHMTLVMFVQTFFGVGLATLFAWIA 139
Valginolyticus_12G01                MLLMNDWSNVWVMSFMSAIFLHILLVHVTRVMFAQTFAGIGLATFFAWVA 139
Vibrio_sp_Ex25                      MLLMNDWSNVWVMSFMSAIFLHILLVHVTRVMFAQTFAGIGLATFFAWVA 139
Vibrio_parahaemolyticus_RIMD_2      MLLMNDWSNVWVMSFMSAIFLHILLVHVTRVMFAQTFAGIGLATFFAWIA 139
Vibrio_parahaemolyticus_AQ3810      MLLMNDWSNVWVMSFMSAIFLHILLVHVTRVMFAQTFAGIGLATFFAWIA 119
Photobacterium_profundum_SS9        MLIMNNWSTVWLMSFMSAIFLHILLVHTTRVMFTQTIVGITLAIVYAWIA 142
Photobacterium_profundum_3TCK       MLIMNNWSTVWLMSFMSAIFLHILLVHTTWVMCTQAIIGIALAVVCAWIA 142
Legionella_pneumophila_str_Cor      LFLMNQASVISAMSLLCGVFLLVLLV-DLLSLSIVLILGFSLALVSYYLV 149
                                    : : *. :    ** :  :*:  *::     :      ..  .

Chlorobium_ferrooxidans_DSM_13      DGRVSFTYFIPEYIPIFIFSIAGSIIASHKQQQAYKS------------ 180
Chlorobium_phaeobacteroides_DS      DGEVSFAFFQLEYIPVFLFSFIGSIIANHNRQLAHQT------------ 180
Chlorobium_limicola_DSM_245         DGHVSYTEFHIEYIPTYLFALIGGIVANHRKQIAHQT------------ 180
Vibrio_angustum_S14                 HPINSD-NFHWGYIAVISFSYVTGIASHYRNHIHYEDQL----------- 180
Photobacterium_sp._SKA34            HPINSD-NFHWGYIAVISFSYVTGIASHYRNHIHYEDQL----------- 180
Vcholerea_C6706str                  TDFHPTTLIEWQYIPIFLFTYVFGNLCFFRNQISHET------------ 180
Vcholerae_1587                      TDFHPTTLIEWQYIPIFLFTYVFGNLCFFRNQISHET------------ 180
Vcholerae_V51                       TDFHPTTLIEWQYIPIFLFTYVFGNLCFFRNQISHETKVSIAKTFGAGIA 169
Vibrio_shilonii_AK1                 GGQGIYMEQSLTYLPIFAFTYIFGSLFFFRNQNEHESKFAIAKSFGAGIA 169
Vibrio_sp_MED222                    QGFYLELTMDWTHVPIFLFIYLFGNLFYFRNQVEHENKVSL--------- 180
Vibrio_splendidus_12B01             QGFYLELTMDWTHVPIFLFIYLFGNLFYFRNQMEHENKVSL--------- 180
Vibrionales_bacterium_SWAT-3        QGFYLEITMNWTHVPIFLFIYLFGNLFYFRNQVEHENKVSL--------- 180
Vibrio_harveyi_ATCC_BAA-1116        QGFHLELTMDWTHVPIFLFIYLFGNLFYFRNQVEHEAKVSI--------- 180
Vibrio_harveyi_HY01                 QGFHLELTMDWTHVPIFLFIYLFGNLFYFRNQVEHEAKVSIAKSFGAGIA 169
Vibrio_campbellii_AND4              QGFHLEYTMDWTHVPIFLFIYLFGNLFYFRNQVEHEAKVSI--------- 180
Valginolyticus_12G01                KGFHLDLTMDWTHVPIFLFIYVFGNLFYFRNQVEHEAKVSL--------- 180
Vibrio_sp_Ex25                      KGFHLDLTMDWTHVPIFLFIYVFGNLFYFRNQVEHEAKVSL--------- 180
Vibrio_parahaemolyticus_RIMD_2      KGFHLDITMDWTHVPIFLFIYVFGNMFYFRNQVEHEAKVSL--------- 180
Vibrio_parahaemolyticus_AQ3810      KGFHLDITMDWTHVPIFLFIYVFGNMFYFRNQVEHEAKVSLAKSFGAGIA 169
Photobacterium_profundum_SS9        KGFSLDVAFDWNHIPIFLFTYIFGNAFYLRNQVEHETK------------ 180
Photobacterium_profundum_3TCK       QSFSLDIALDWSHMPIFLFTYIFGNAFYLRNQVEHETK------------ 180
Legionella_pneumophila_str_Cor      SPQMYFGEEHIQMTLVIIFTIIAGSTLNYKT------------------- 180
                                                        *    .     .
```

Table 1. CqsS mutant phenotypes[a]

Allele	Phenotype[b]	CAI-1 EC_{50} (M)	CAI-1 EC_{50} 95%CL[c] (M)	Amino CAI-1 EC_{50} (M)	Amino-CAI-1 EC_{50} 95%CL (M)	Estimated $K_{off/CAI-1}$ compared with wild type[cd]
WT	W	3.5×10^{-7}	$3.2\text{-}3.9 \times 10^{-7}$	1.2×10^{-7}	$1.2\text{-}1.3 \times 10^{-7}$	
G29A	W	2.1×10^{-7}	$1.8\text{-}2.6 \times 10^{-7}$	1.0×10^{-7}	$0.9\text{-}1.1 \times 10^{-7}$	ND
P31A	P	2.5×10^{-8}	$2.3\text{-}2.8 \times 10^{-8}$	7.7×10^{-9}	$7.2\text{-}8.1 \times 10^{-9}$	L
W37A	K	ND		ND		ND
P42A	W	4.0×10^{-7}	$3.2\text{-}5.0 \times 10^{-7}$	1.4×10^{-7}	$1.2\text{-}1.5 \times 10^{-7}$	ND
Q43A	K	2.5×10^{-6}	$1.8\text{-}3.3 \times 10^{-6}$	6.5×10^{-7}	$5.9\text{-}7.1 \times 10^{-7}$	H
Y45A	W	2.5×10^{-7}	$2.0\text{-}3.2 \times 10^{-7}$	1.2×10^{-7}	$1.1\text{-}1.2 \times 10^{-7}$	ND
E46A	K	4.0×10^{-6}	$3.2\text{-}5.0 \times 10^{-6}$	2.6×10^{-6}	$2.2\text{-}3.1 \times 10^{-6}$	H
R51A	K	ND		ND		ND
P88A	W	8.7×10^{-7}	$7.5\text{-}10 \times 10^{-7}$	1.8×10^{-7}	$1.7\text{-}1.9 \times 10^{-7}$	ND
F90A	W	1.3×10^{-7}	$1.0\text{-}1.6 \times 10^{-7}$	6.0×10^{-8}	$5.0\text{-}7.2 \times 10^{-8}$	ND
F91A	K	2.8×10^{-6}	$2.4\text{-}3.3 \times 10^{-6}$	3.0×10^{-6}	$2.6\text{-}3.5 \times 10^{-6}$	H
N98A	W	3.8×10^{-7}	$3.3\text{-}4.4 \times 10^{-7}$	1.3×10^{-7}	$1.2\text{-}1.4 \times 10^{-7}$	ND
W104A	S	1.1×10^{-7}	$1.0\text{-}1.2 \times 10^{-7}$	4.3×10^{-7}	$4.1\text{-}4.6 \times 10^{-7}$	L
M106A	W	3.1×10^{-7}	$2.9\text{-}3.3 \times 10^{-7}$	1.0×10^{-7}	$1.0\text{-}1.1 \times 10^{-7}$	ND
S107A	S	2.2×10^{-7}	$1.7\text{-}2.7 \times 10^{-7}$	5.8×10^{-7}	$5.1\text{-}6.6 \times 10^{-7}$	L
F113A	K	4.9×10^{-6}	$3.8\text{-}6.4 \times 10^{-6}$	1.2×10^{-6}	$1.1\text{-}1.3 \times 10^{-6}$	H
L117A	W	3.1×10^{-7}	$2.8\text{-}3.4 \times 10^{-7}$	9.1×10^{-8}	$8.6\text{-}9.6 \times 10^{-8}$	ND
F162A	K/S	ND		ND		ND
W104A/S107A	S	4.7×10^{-8}	$4.5\text{-}4.9 \times 10^{-8}$	1.7×10^{-6}	$1.5\text{-}1.8 \times 10^{-6}$	L

[a] ND, not determined. [b] Phenotypes of mutants. W, wild type, insignificant change in sensitivity of the receptor; P, phosphatase-biased, more sensitive to CAI-1, K, kinase-biased, less sensitive to CAI-1; S, specificity mutants, changes the specificity of the receptor to prefer CAI-1 over amino-CAI-1. [c] 95% Confidence Intervals. [d] Estimated $K_{off/CAI-1}$ values compared with wild type. H, higher than wild type; L, lower than wild type. See S3 for a detailed analysis. Experiments were performed at least three times.

S3. Automated program for data collapse

Dose-response curves for wild-type CqsS and various CqsS mutants were obtained by changing the concentration of agonist (CAI-1 or amino-CAI-1) while fixing the antagonist phenyl-CAI-1 at four different concentrations (0, 16, 32, and 64 μM) to produce a set of four distinct dose-response curves for each type of agonist (see Figure S1A for wild-type CqsS response to CAI-1 and amino-CAI-1). For four strains (wild-type, W104A, W104A/S107A, S107A) dose-response curves were obtained using both CAI-1 and amino-CAI-1; for all other strains dose-response curves were obtained using only CAI-1 (Table S1). These multiple dose-response curves, including both agonists and competitive antagonists for each strain, allowed us to use a method of data collapse (1) to infer the underlying biochemical and biophysical parameters of each CqsS mutant and to better understand the properties of the ligand-binding pocket interaction.

The principle underlying the collapse of dose-response data is that there exists a fixed quantitative relation between measured Qrr4-GFP fluorescence intensity (GFP) and the free-energy difference f between the kinase active and inactive configurations of CqsS, as defined in the main text Equation (1) (1, 2). Therefore, all data from various dose-response curves of the same CqsS mutant strain should reproduce this same relation, i.e., the curves should "collapse" when GFP fluorescence is plotted versus the free-energy difference f .

To plot data in this way, we need to know how to relate ligand concentrations to free-energy differences. According to Equation (1) in the main text, we need to know the ligand dissociation constants $K_{\text{off/on}}^{\text{CAI-1/Ant}}$ as well as the free-energy difference $\Delta\varepsilon$ between "on" and "off" states at zero ligand concentration.

In practice, we automated the search for dissociation constants $K_{\text{off/on}}^{\text{CAI-1/Ant}}$ by assuming the following simple functional form for the quantitative relation between GFP and free-energy difference:

$$\text{GFP} = b + \frac{a-b}{1+\exp\left[\left(E-u\right)\cdot h\right]}, \tag{S1}$$

where

$$E = f - \Delta\varepsilon = \log\left(\frac{1+\frac{[\text{CAI-1}]}{K_{\text{off}}^{\text{CAI-1}}}}{1+\frac{[\text{CAI-1}]}{K_{\text{on}}^{\text{CAI-1}}}}\right) + \log\left(\frac{1+\frac{[\text{Ant}]}{K_{\text{off}}^{\text{Ant}}}}{1+\frac{[\text{Ant}]}{K_{\text{on}}^{\text{Ant}}}}\right) \quad \text{(S2)}$$

and where a is the upper plateau of GFP intensity (in the low free-energy limit, $E \to -\infty$), b is the lower plateau of GFP intensity (in the high free-energy limit, $E \to +\infty$), and u determines the center and h determines the maximum slope of the sigmoidal curve relating GFP to the free-energy difference.

In our automated computer program, $K_{\text{off/on}}^{\text{CAI-1/Ant}}$, a, b, u, and h are considered as unknown parameters and their values are explored in a wide range to achieve the best collapse of the data. The "best collapse" is identified by minimizing the sum of squared deviations from the single curve described in Equation (S1) for all data points in various dose-response curves, i.e. the "best collapse" has the tightest spread of data points around the collapsed curve:

$$\min_{K_{\text{off/on}}^{\text{CAI-1/Ant}},a,b,u,h} \sum_i \left(\overline{\text{GFP}_i} - \text{GFP}_i\right)^2, \quad \text{(S3)}$$

where $\overline{\text{GFP}_i}$ is the measured GFP intensity of data point i (i ranges over the total number of data points in the set of dose-response curves), and GFP_i is calculated according to Equations (S1) and (S2) using the actual ligand concentrations for data point i and the proposed parameter values for the single data-collapse curve (Equation (S1)). The program starts with an estimated set of parameters and iteratively improves the estimates for all the parameter values by optimizing the objective function in Equation (S3) using the Matlab® optimization toolbox (source code available upon request). This is expected to be a reliable procedure in our case because the dose-response curves contain more data than the number of unknown parameters.

In practice, we first determined the h value for wild-type CqsS and all CqsS mutants. We assumed the slope of the quantitative relation between GFP and free-energy difference should be consistent regardless of mutations in CqsS since this slope is a property only of the downstream signaling pathway. (This assumption will hold provided mutations only affect the balance between the on and off states of CqsS, not its catalytic

rate constants or overall abundance.) h was increased from -4 to -2 in steps of 0.1. At each specified h value, all other parameters were optimized to yield a minimal residue over all strains (Equation (S3)). The minimum of the sum of residues occurred for $h = -2.7$, and we took this value as our best collapse estimate (Figure S2A). Next we determined the best collapse values of the energy shift u for wild-type CqsS and for each CqsS mutant separately. For each of these CqsS proteins, the free-energy difference at zero ligand concentration $\Delta\varepsilon$ should be independent of ligand type (either CAI-1 or amino-CAI-1) and of antagonist concentration. (Any additional shift of the center of the sigmoidal function (S1) away from $f = 0$ arising from the downstream pathway should also be a constant for all strains.) Therefore, for each strain, we searched for the best collapse u by increasing u from 0 to 2 in steps of 0.1 with h fixed at -2.7. At each specified u value, the remainder of the parameters were optimized over the CAI-1 and amino-CAI-1 dose-response data. For each strain, the best estimate of u was determined as the one corresponding to the minimal sum of residues (an example for wild-type CqsS is shown in Figure S2B).

Once the global h value and the u values for each strain were determined, the rest of the parameters were optimized; these are listed in Table S1. An example of dose-response curves after data collapse is shown in Figure S1B for wild-type CqsS.

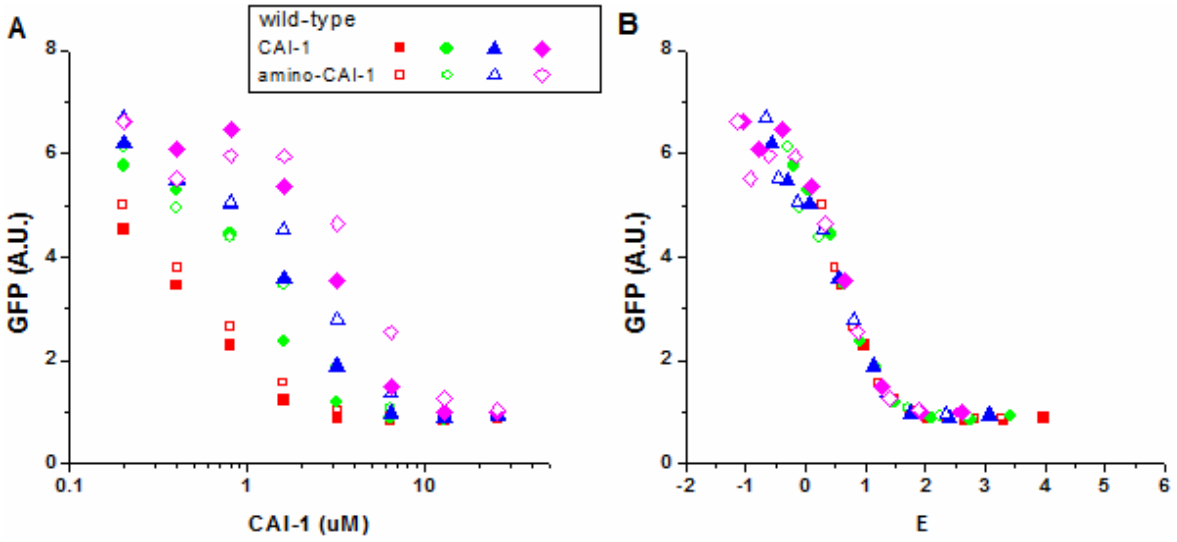

Figure S1. Dose-response curves for wild-type CqsS induced with CAI-1 and amino-CAI-1 (A) before and (B) after data collapse. Each dose-response curve was obtained by varying the concentration of CAI-1 (solid symbols) or amino-CAI-1 (open symbols) while fixing phenyl-CAI-1 at four different concentrations: 0 μM (red), 16 μM (green), 32 μM (blue), and 64 μM (purple).

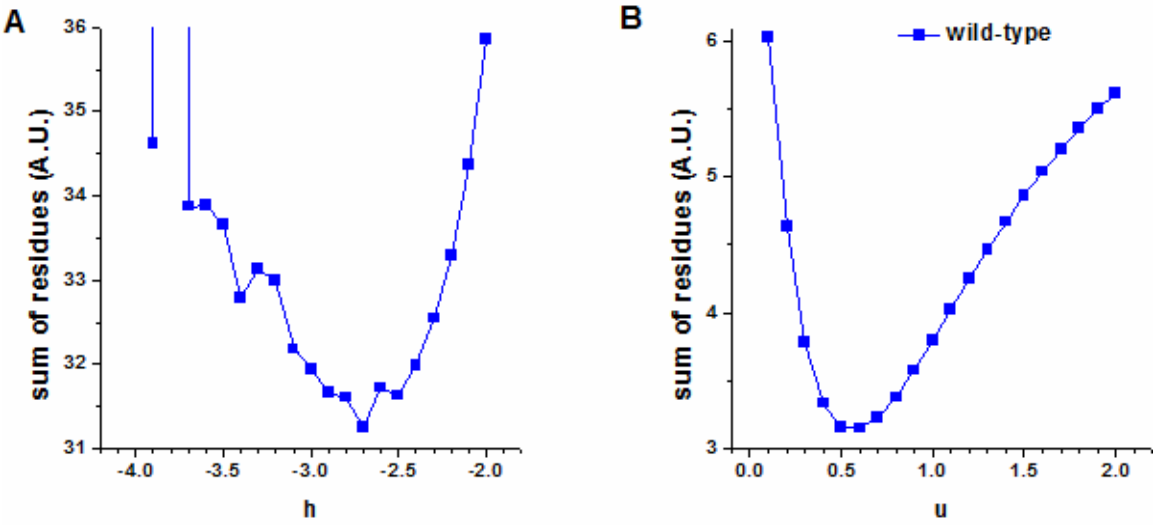

Figure S2. Optimization of parameters h and u for data collapse. (A) The h value was increased from -4 to -2 in steps of 0.1. At each specified h, all other parameters were optimized for individual strains to yield a minimal residue. The minimum sum of residues occurred at $h = -2.7$, and that value is taken as the best estimate for h. (B) As an example, for the wild-type CqsS strain we searched for the best collapse u by increasing u from 0 to 2 in steps of 0.1 with h fixed at -2.7. At each specified u value, the rest of parameters were optimized over the CAI-1 and amino-CAI-1 dose-response data. The best estimate of u in this case occurred at 0.6 where the sum of residues is minimized.

Strain	K_{off}^{CAI-1} (μM)	K_{on}^{CAI-1} (μM)	K_{off}^{Ant} (μM)	K_{on}^{Ant} (μM)	*a*	*b*	*u*	*h*
WT	0.48	9.9×10^{2}	1.0×10^{5}	21	6.41	0.84	0.6	-2.7
WT a	0.31	23	1.3×10^{4}	20	6.23	0.84	0.6	-2.7
W104A	0.02	10	1.4×10^{4}	8.7	5.8	0.78	1.3	-2.7
W104A a	0.20	2.3×10^{4}	6.8×10^{2}	7.9	6.6	0.87	1.3	-2.7
W104A/S107A	0.01	1.9	2.6×10^{2}	5.6	6.2	0.78	0.9	-2.7
W104A/S107A a	0.90	1.3×10^{5}	1.2×10^{2}	1.6	6.4	0.89	0.9	-2.7
S107A	0.28	1.6	91	20	7.7	1.0	0.2	-2.7
S107A a	3.6	23	1.6×10^{2}	30	7.6	0.9	0.2	-2.7
G29A	0.14	1.0×10^{6}	5.0×10^{4}	93	5.0	0.83	1.3	-2.7
P31A	0.02	0.60	4.5×10^{2}	32	3.4	0.82	0.9	-2.7
Q43A	2.4	19	3.6×10^{2}	43	5.8	1.1	0.5	-2.7
E46A	5.8	38	1.0×10^{3}	69	6.3	2.0	0.6	-2.7
F91A	3.4	1.0×10^{6}	5.0×10^{4}	11	4.8	1.1	1.1	-2.7
N98A	0.82	2.1×10^{4}	1.0×10^{3}	29	6.3	0.81	0.6	-2.7
F113A	3.9	1.6×10^{2}	1.0×10^{4}	50	6.6	0.84	0.6	-2.7

Table S1. List of parameters estimated from best collapse of dose-response data for all strains. "a" : amino-CAI-1.

References:

1. Swem LR, Swem DL, Wingreen NS, & Bassler BL (2008) Deducing receptor signaling parameters from in vivo analysis: LuxN/AI-1 quorum sensing in *Vibrio harveyi*. *Cell* 134:461-473.
2. Keymer JE, Endres RG, Skoge M, Meir Y, & Wingreen NS (2006) Chemosensing in *Escherichia coli*: two regimes of two-state receptors. *Proc Natl Acad Sci U S A* 103:1786-1791.

S4. W104 and S107 specify the preference for the C3 moiety of CAI-1

We constructed additional mutants at W104 and S107 to probe the functions of these two residues. CqsS S107C, CqsS W104F, and CqsS W104Y prefer CAI-1 to amino-CAI-1. By contrast, CqsS S107T retains the wild type CqsS preference for the two autoinducers while it also decreases sensitivity to both molecules. Closed circles, CAI-1; Open circles, amino-CAI-1.

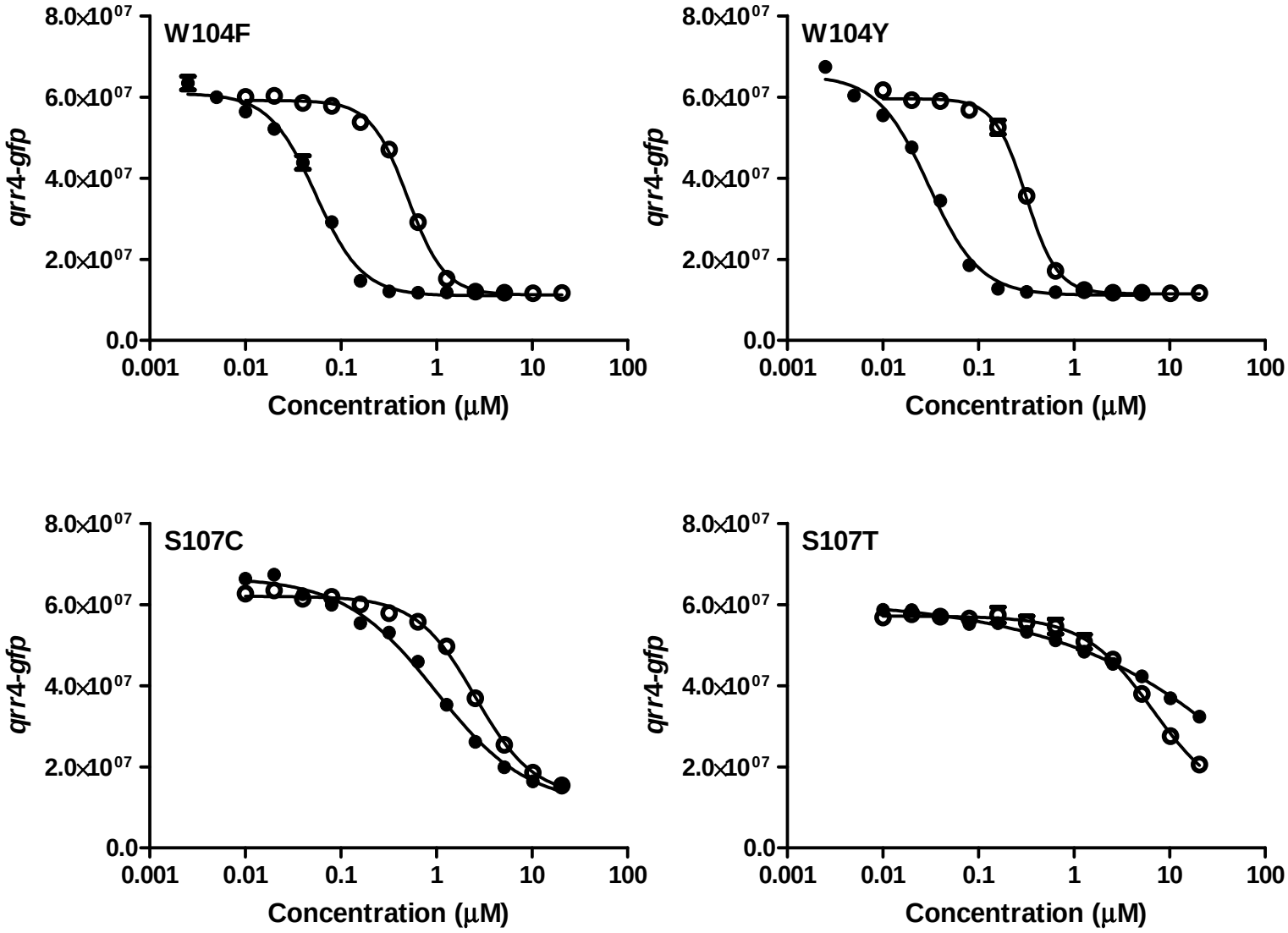

S5. P-CAI-1 is a competitive antagonist and P-CAI-1 sensing mutants

To test whether P-CAI-1 acts a competitive antagonist of CAI-1, the *qrr*4-*gfp* response to various concentrations of CAI-1 was assayed in the presence of 0, 16, 64, and 256 μM of P-CAI-1. Increasing concentrations of P-CAI-1 increase the EC_{50} values of CAI-1 for *qrr*4-*gfp* repression, while increasing concentrations of CAI-1 alleviate antagonism.

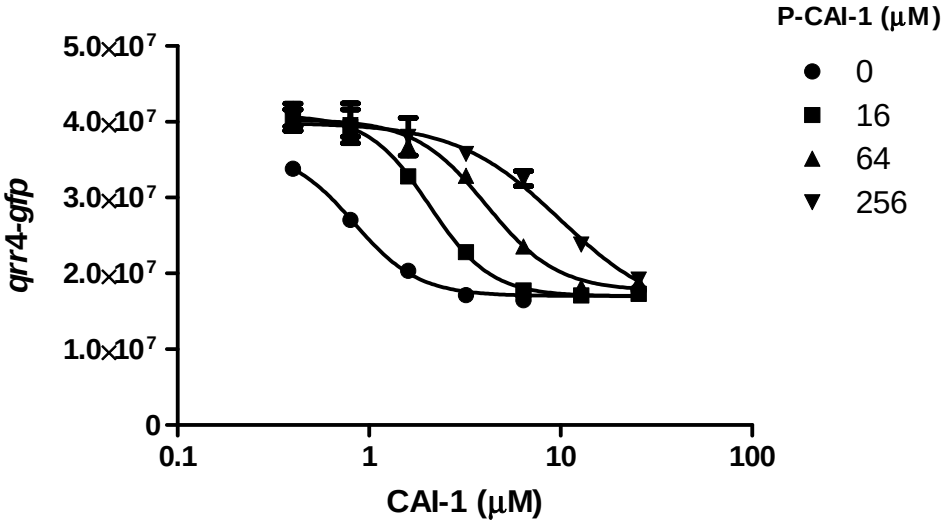

S6A. CqsS M106A and CqsS F166L responses to CAI-1 and P-CAI-1

In addition to CqsS F160I and CqsS F162 (see main manuscript text), we identified two CqsS mutants (M106A and F166L) that respond to P-CAI-1. CqsS M106A responds to both CAI-1 and P-CAI-1. CqsS F166L responds to P-CAI-1 and has reduced sensitivity to CAI-1. Wild type CqsS is shown for reference.

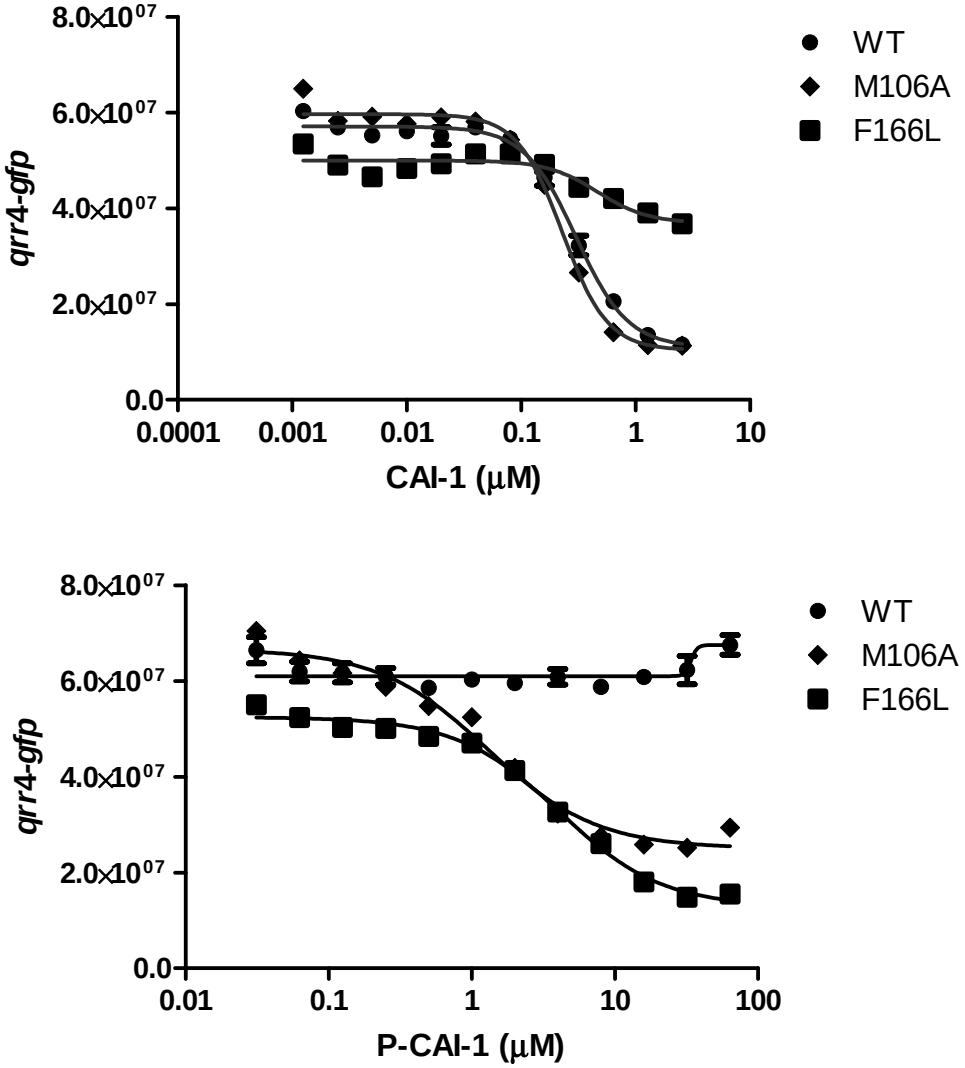

S6B. The F162A mutation is epistatic to other point mutations for the CAI-1 response

When combined with other mutations, F162A renders the resulting CqsS double mutants insensitive to CAI-1. The CqsS F160I/F162A mutant is shown as an example in the main text, here, we show that CqsS M106A/F162A, CqsS F160I/F162A, and CqsS F162A/F166L are all also insensitive to CAI-1. The wild type response is shown for reference.

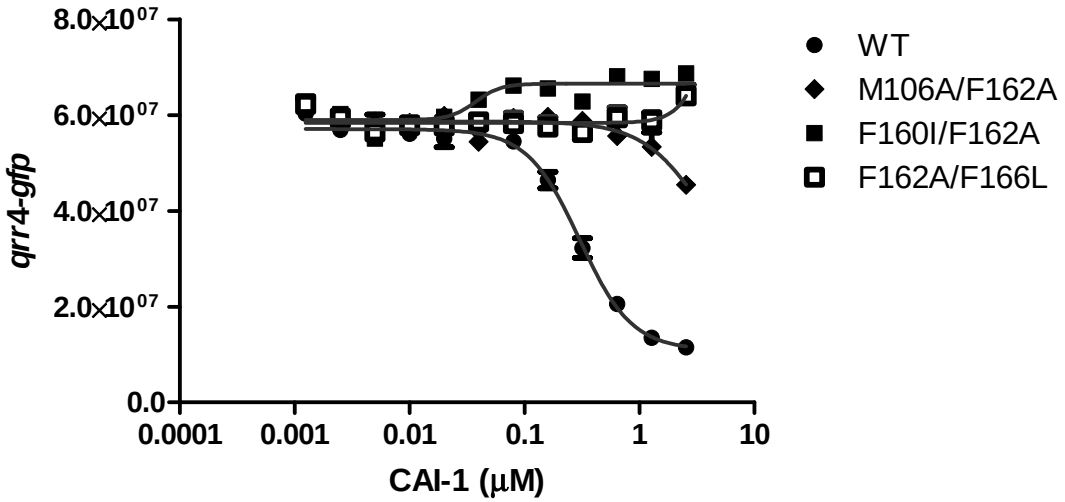

S7A. CqsS mutant responses to C8-CAI-1

In addition the CqsS M106A mutant described in the main text, we identified CqsS W104A, L117A, M125A mutants that respond to C8-CAI-1 without significantly changing the sensitivity to CAI-1. Wild type is shown for reference.

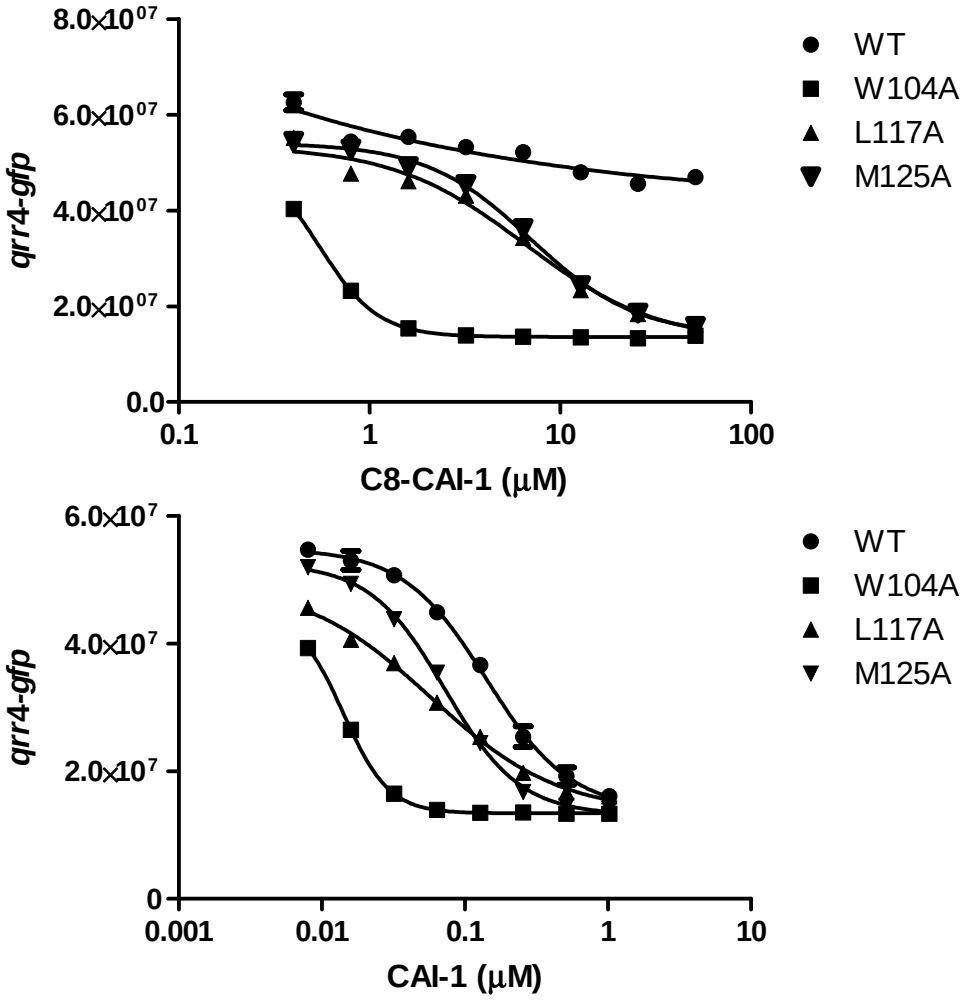

S7B. C170 determines CAI-1 tail length preference

Responses to CAI-1 and C8-CAI-1 are determined in wild type and mutants with alterations at position 170. Strains with small residues in position 170, as in wild type and CqsS C170A, prefer CAI-1 as an agonist, while stains with bulky residues in position 170 as in CqsS C170Y and CqsS C170F prefer C8-CAI-1 as an agonist.

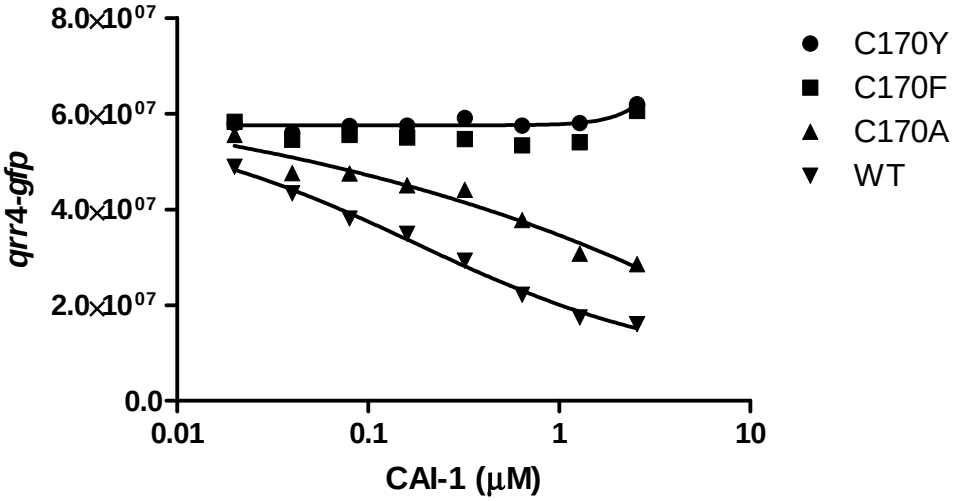

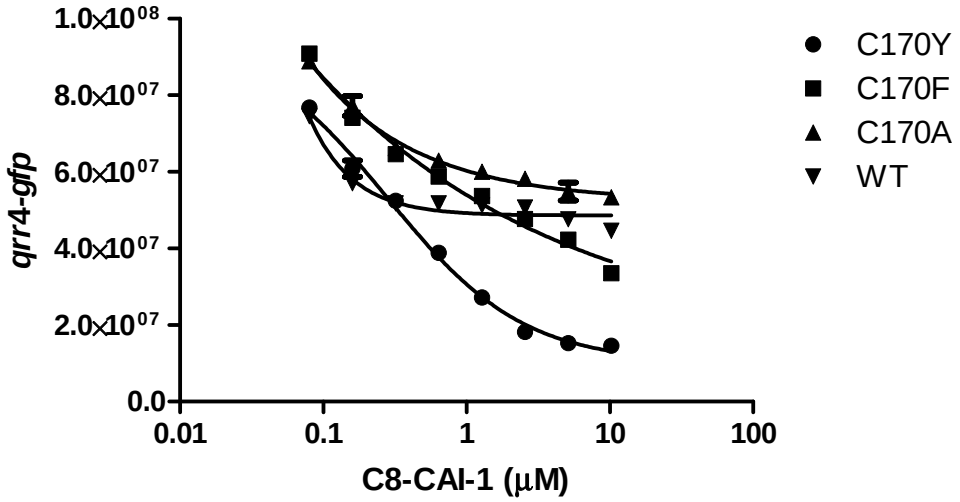

S7C. **CAI-1 acts as a competitive antagonist of the CqsS C170Y mutant**

To test whether CAI-1 acts a competitive antagonist for the CqsS C170Y mutant that only responds to C8-CAI-1, the *qrr*4-*gfp* response to various concentrations of C8-CAI-1 was determined in the presence of 0, 0.64, 2.56 and 10.24 μM of CAI-1. Increasing concentrations of CAI-1 increase the EC_{50} value of C8-CAI-1 for *qrr*4-*gfp* repression, while increasing concentrations of C8-CAI-1 alleviate CAI-1 antagonism.

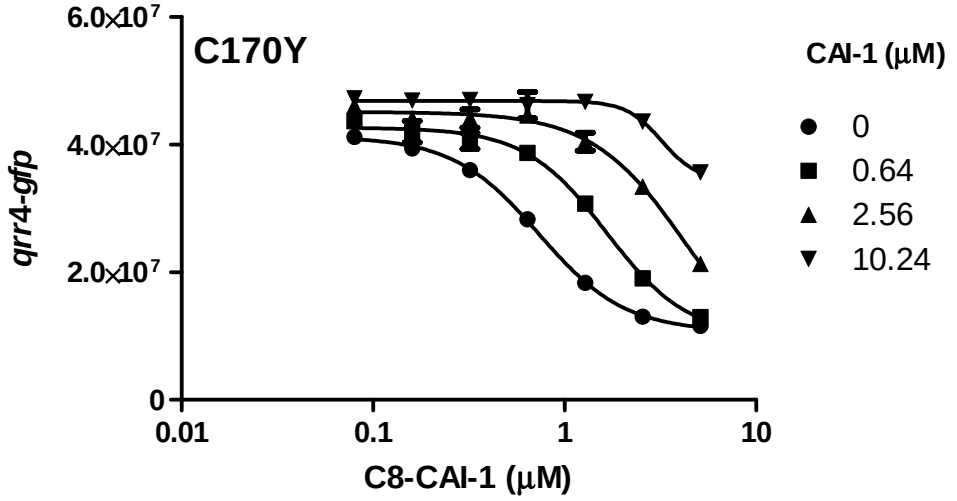

S8. Phylognetic analysis of CqsA and CqsS homologs in different *vibrios*

Phylogenetic trees were built with full length *cqsA* and *luxS* sequences. Only the portions of the genes encoding the transmembrane regions of *cqsS* were used to assemble the *cqsS* phylogenetic tree. We find that the organization of the *cqsA* and *cqsS* phylogenetic trees is similar, while the *luxS* tree varies.

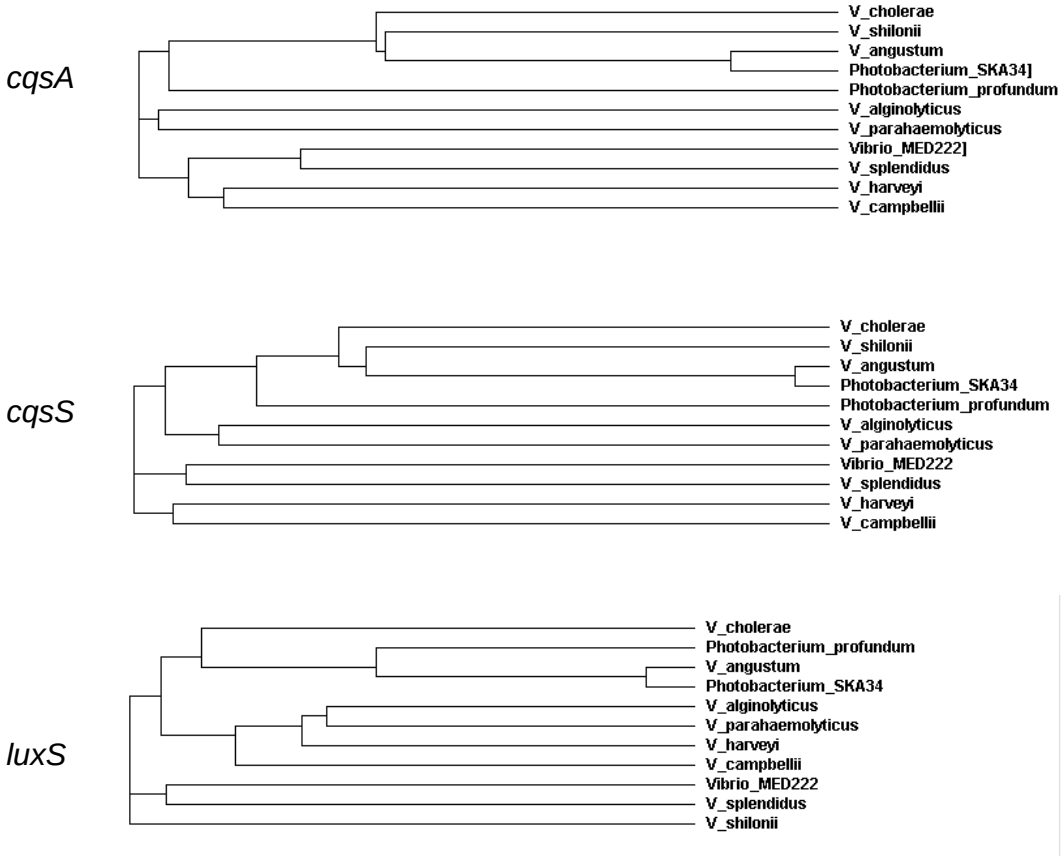

S9. Materials and Methods

Bacterial strains and media

V. cholerae strains were derived from *V. cholerae* C6706str2 (1) and grown in LB broth aerobically at 30 ^{o}C. Plasmids were maintained in *E. coli* strain DH10B or XL10Gold at 37 ^{o}C in LB broth with appropriate antibiotics. Triparental matings were performed with the helper plasmid pRK2013 as described (2). When needed, kanamycin (Kan) was added to a final concentration of 100 μg/ml, polymyxin was added to a final concentration of 50 units/ml. A list of strains and plasmids used in this study is listed below.

The following *V. cholerae* strains are derivatives of DH245 (Δ*cqsA* Δ*cqsS* Δ*luxQ*). Each strain carries a plasmid containing the *qrr*4-*gfp* transcriptional fusion and a different *cqsS* allele.	
Strain	Allele
WYZ406	WT
WYZ422	G29A
WYZ424	P31A
WYZ400	W37A
WYZ426	P42A
WYZ428	Q43A
WYZ430	Y45A
WYZ432	E46A
WYZ434	R51A
JC1505	P88A
JC1493	F90A
JC1494	F91A
JC1506	N98A
WYZ527	W104A
WYZ664	W104F
WYZ665	W104Y
JC1507	M106A
WYZ479	S107A
WYZ494	S107C
WYZ666	S107T
JC1495	F113A
JC1510	L117A
JC1509	F162A
WYZ715	P31A/F91A
WYZ591	W104A/S107A
WN1231	F160I
WN1225	F166L
WN1366	C170Y

WN1367	C170F
WN1428	C170A
WN1457	M106A/F160I
WN1474	M106A/F162A
WN1417	F160I/F162A
WN1433	F162A/F166L
WN1277	F160I/F166L
WN1430	F162A/C170Y
WN1449	F166L/C170Y

DNA manipulation and plasmid construction

DNA manipulations were performed using standard methods as described (3). Site-directed mutagenesis was performed with the Quikchange II XL Site-Directed Mutagenesis Kit (Stratagene). Sequential 3' random deletions to generate *cqsS-lacZ* and *cqsS-phoA* fusions were performed with the Erase-a-base System (Promega). The *cqsS-lacZ* translational fusion was constructed in plasmid pRS414 (4). The portion of *cqsS* encoding the first 185 N-terminal residues and the endogenous promoter was amplified by primers Vc960 and WN1465, and the resulting PCR product was digested with *Eco*R I and *Bam*H I and cloned into pRS414 digested with the same enzymes. The *cqsS-phoA* translational fusion was constructed in plasmid pEVS143 (5) with a three-fragment ligation. *cqsS* encoding the first 185 N-terminal residues was amplified by primers Vc946 and WN1466 and digested with *Xba* I and *Not* I. *phoA* from *E. coli* lacking the first 26 amino acids was amplified by primers AP121 and AP123 and digested with *Not* I and *Bam*H I. The two digested PCR products were ligated simultaneously to pEVS143 digested with *Avr* II and *Bam*H I. For pDH345 construction, *cqsS* was cloned with a C-terminal FLAG tag into pEVS143 under the control of P_{tac} promoter to obtain plasmid pDH251. We next PCR amplified the P_{tac}-*cqsS* together with *lacI* from pDH251 into the *Bam*H I site of the previously reported plasmid pSLS4 (6), which carries the *qrr*4-*gfp* transcriptional fusion. Primer sequences are available upon request.

***cqsS* random mutant library construction**

The portion of *cqsS* encoding the N-terminal 173 residues cloned into pDH345 was subjected to random mutagenesis by error prone PCR using GeneMorph II EZClone Domain Mutagenesis Kit. The resulting mutagenized fragments of *cqsS* were used as

megaprimers to fuse with the remaining unmutagenized portion of *cqsS* according to the manufacturer's instructions. This yielded clones averaging 2-3 bp changes. This *cqsS* mutant plasmid library was conjugated into *V. cholerae* Δ*cqsA* Δ*cqsS* Δ*luxQ* strain DH245. Exoconjugants were selected on LB medium with polymyxin and kanamycin. Individual clones were arrayed into 96-well plates and used for subsequent screening. In each screen, several thousand clones were assessed for sensitivity to CAI-1 and analogs using the *qrr*4-*gfp* assay described below. Candidate plasmids were isolated and *cqsS* was sequenced to map the mutations. Individual mutations were engineered by site-directed mutagenesis in pDH345 and re-introduced to DH245 to verify phenotypes. Western blotting using anti-FLAG antibodies was performed to ensure that mutant CqsS production was comparable to wild type.

***qrr*4-*gfp* reporter assay**

Dose-response curves were generated in *V. cholerae* DH245 carrying plasmid pDH345 harboring wild type or mutant *cqsS. S*trains were grown overnight at 30 ^{o}C in LB broth with kanamycin and diluted 1:50 in the identical medium containing different concentrations of either CAI-1 or a CAI-1 analog in triplicate or quadruplicate in 96-well plates. GFP fluorescence and optical density were measured after 6-8 h incubation using an Envision 2103 Multilabel Reader (Perkin Elmer). Non-linear curve fitting was used to determine the EC_{50} values using GraphPad Prism software.

CqsS free energy model and automated data collapse

Similar to the receptor kinase LuxN in *V. harveyi* (7), CqsS is considered to switch between its kinase active (on) and kinase inactive (off) states. In equilibrium, the probability for a CqsS to be in its kinase active state is determined by the free-energy difference, $f = f_{on} - f_{off}$, between the two states according to $p_{on} = \frac{1}{1+e^{f}}$ (all energies are in units of the thermal energy $k_B T$). Assuming competitive binding of CAI-1 and its antagonist to CqsS, one obtains

$$f = \Delta\varepsilon + \log\left(\frac{1+\frac{[\text{CAI-1}]}{K_{\text{off}}^{\text{CAI-1}}}}{1+\frac{[\text{CAI-1}]}{K_{\text{on}}^{\text{CAI-1}}}}\right) + \log\left(\frac{1+\frac{[\text{Ant}]}{K_{\text{off}}^{\text{Ant}}}}{1+\frac{[\text{Ant}]}{K_{\text{on}}^{\text{Ant}}}}\right), \quad (1)$$

Where $K_{\text{off/on}}^{\text{CAI-1/Ant}}$ is the dissociation constant for the given state and ligand and $\Delta\varepsilon$ is the free energy difference of "on" and "off" states at zero ligand concentration (7, 8).

We assume that *qrr*4-*gfp* expression is some (unknown) function of the fraction of CqsS proteins in the kinase active (on) state. Therefore, when we plot Qrr4-GFP intensity as a function of f, all data points in different dose-response curves for the same CqsS mutant should collapse onto a single curve. We designed an automated computer program to search for the values of $K_{\text{off/on}}^{\text{CAI-1/Ant}}$ which best collapse all data onto one single curve in a GFP versus f plot (see Supplemental Information S3 for more details).

Chemical and analytical methods

All compounds are prepared as racemic mixtures at the C3 position. Previous studies showed that both *S*- and *R*-forms of CAI-1 are detected by CqsS (9).

3-hydroxytridecan-4-one, CAI-1. Prepared according to the previously reported procedure (9). ^{1}H NMR (500 MHz, $CDCl_3$) δ 4.13 (td, J = 6.7, 4.5 Hz, 1H), 3.51 (d, J = 4.9 Hz, 1H), 2.57-2.30 (m, 2H), 1.92-1.85 (m, 1H), 1.64-1.53 (m, 3H), 1.34-1.19 (m, 12H), 0.91 (t, J = 7.4 Hz, 3H), 0.85 (t, J = 6.9 Hz, 3H); ^{13}C NMR (125 MHz, $CDCl_3$) δ 212.4, 77.1, 37.8, 31.8, 29.3, 29.3, 29.2, 26.7, 23.5, 22.6, 14.0, 8.8; HRMS (ESI-TOF) calcd. for $C_{13}H_{27}O_2$ $[M+H]^+$, 215.2011; found, 215.2013 $[M+H]^+$.

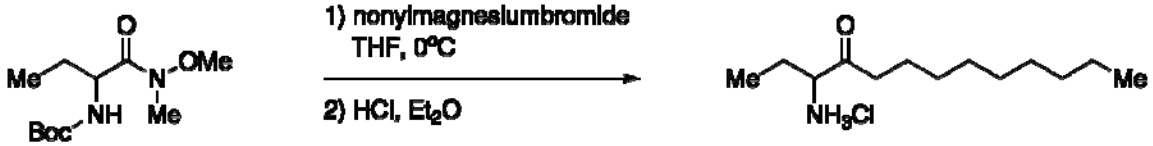

3-aminotridecan-4-one hydrochloride, Amino-CAI-1. The known Weinreb amide, *tert*-butyl 1-(methoxy(methyl)amino)-1-oxobutan-2-ylcarbamate (200mg, 0.812 mmol)

(10) in THF was added to a freshly prepared, cooled (0 ^{o}C) solution of nonylmagnesium bromide (Prepared from 1-bromononane (1.5 mL, 8.1 mmol) and Mg^{0} (207 mg, 8.53 mmol) in THF (16 mL).) dropwise via syringe. The mixture was allowed to stir for 3.5 h at 0 ^{o}C with monitoring by TLC. Upon consumption of starting material the reaction was quenched by the addition of sat. NH_4Cl, was extracted with Et_2O, dried over Na_2SO_4, filtered and concentrated. The residue was purified by flash column chromatography (hexanes to 40% EtOAc/hexanes) and was used without further purification. This intermediate was dissolved in Et_2O (1.5 mL), was treated with HCl (560 µL, 1.12 mmol, 2.0M in Et_2O) at r.t., was allowed to stir at r.t. for 14 h and was concentrated *in vacuo* to provide a yellow waxy solid (168.4 mg, 83% two steps). Further purification could be achieved by recrystallization from a minimal amount of $CHCl_3$ at 0 ^{o}C to provide finely dispersed white crystals. ^{1}H NMR (500 MHz, D_2O) δ 4.11 (dd, *J* = 7.1, 4.4 Hz, 1H), 2.49 (m, 2H), 1.97 (ddd, *J* = 15.1, 7.6, 4.5 Hz, 1H), 1.87 (dt, *J* = 15.1, 7.5 Hz, 1H), 1.12 (m, 12H), 1.43 (m, 2H), 0.84 (t, *J* = 7.5 Hz, 3H), 0.79 (t, *J* = 6.8 Hz, 3H); ^{13}C-NMR (125 MHz, DMSO-*d*6) δ 207.0, 58.9, 38.3, 31.4, 28.9, 28.9, 28.7, 28.5, 22.8, 22.5, 22.2, 14.1, 8.9; HRMS (ESI-TOF) calcd. for $C_{13}H_{28}NO$ $[M\text{-}Cl]^{+}$, 214.2171; found 214.2168 $[M\text{-}Cl]^{+}$.

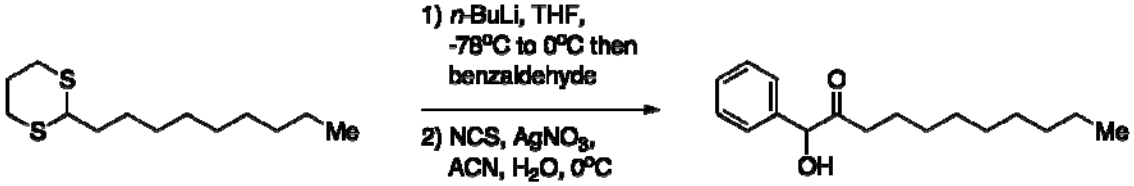

1-hydroxy-1-phenylundecan-2-one, Phenyl-CAI-1. A solution of 2-nonyl-1,3-dithiane (11) (302 mg, 1.2 mmol) in THF (7.2ml) was cooled to -20 °C, was treated with *n*-butyl lithium (740 µL, 2.5M in hexanes) and allowed to stir for 4 hours. The mixture was cooled to -78 °C, benzaldehyde (125 µL, 1.2 mmol, 1M in THF) was added dropwise and the reaction mixture was allowed to warm to room temperature overnight. The reaction was quenched with sat. NH_4Cl, extracted with Et_2O (2 x 50mL), washed with brine, dried over Na_2SO_4, filtered, concentrated and purified by silica gel column chromatography providing (2-nonyl-1,3-dithian-2-yl)(phenyl)methanol which was used without further purification. This product was dissolved in ACN (1.2 mL) and was added to a cooled

(0°C) solution of *N*-chlorosuccinimide (657 mg, 4.9 mmol) and $AgNO_3$ (836 mg, 4.9 mmol) in MeCN (7.2 ml) and H_2O (1.4 ml). The mixture was then allowed to warm to room temperature overnight, was quenched with sat. Na_2SO_3 (10 ml), extracted with Et_2O (2 x 50mL), dried over Na_2SO_4, filtered, and concentrated. The residue was purified by silica gel chromatography (hexanes to 10% EtOAc/hexanes) to provide 1-hydroxy-1-phenylundecan-2-one as a white solid (137.8 mg, 43% two steps). ^{1}H NMR (500 MHz, $CDCl_3$) δ 7.27 (m, 5H), 5.01 (d, *J* = 4.4 Hz, 1H), 4.33 (d, *J* = 4.4 Hz, 1H), 2.32-2.20 (m, 2H), 1.46-1.32 (m, 2H), 1.23-0.98 (m, 12H), 0.79 (t, *J* = 5.8 Hz, 3H); ^{13}C NMR (125 MHz, $CDCl_3$) δ 209.7, 138.1, 129.0, 128.7, 127.5, 79.7, 37.8, 31.9, 29.4, 29.2, 28.9, 24.5, 23.7, 22.7, 14.17; HRMS (ESI-TOF) calcd. for $C_{17}H_{26}O_2Na$ $[M+Na]^+$, 285.1830; found, 285.1826 $[M+Na]^+$.

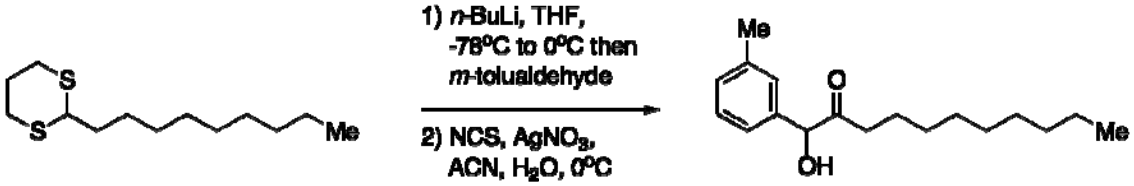

1-hydroxy-1-*m*-tolylundecan-2-one, Methyl-phenyl-CAI-1. A solution of 2-nonyl-1,3-dithiane (11) (1.0 g, 4.1 mmol) in THF (24 ml) was cooled to -20 °C, was treated with *n*-butyl lithium (2.5 mL, 2.5M in hexanes) and allowed to stir for 4 hours. The mixture was cooled to -78 °C, *m*-tolualdehyde (970 μL, 8.2 mmol, 1M in THF) was added dropwise and the reaction mixture was allowed to warm to room temperature overnight. The reaction was quenched with sat. NH_4Cl, extracted with Et_2O (2 x 50mL), washed with brine, dried over Na_2SO_4, filtered, concentrated and purified by silica gel column chromatography providing (2-nonyl-1,3-dithian-2-yl)(*m*-tolyl)methanol which was used without further purification. This product was dissolved in ACN (10 mL) and was added to a cooled (0 °C) solution of *N*-chlorosuccinimide (2.2 g, 16.4 mmol) and $AgNO_3$ (2.8 g, 16.4 mmol) in MeCN (110 ml) and H_2O (20 ml). The mixture was then allowed to warm to room temperature overnight, was quenched with sat. Na_2SO_3 (10 ml), extracted with Et_2O (2 x 50mL), dried over Na_2SO_4, filtered, and concentrated. The residue was purified by silica gel chromatography (hexanes to 10% EtOAc/hexanes) to provide 1-

hydroxy-1-*m*-tolylundecan-2-one (306.2 mg, 27% two steps). ^{1}H NMR (500 MHz, $CDCl_3$) δ 7.27 (m, 1H), 7.13 (m, 3H), 5.07 (s, 1H), 4.37 (s, 1H), 2.37 (m, 5H), 1.51 (m, 2H), 1.22 (m, 12H), 0.87 (t, J = 7.1 Hz, 3H). ^{13}C NMR (125 MHz, $CDCl_3$) δ 210.1, 139.0, 138.2, 129.6, 129.0, 128.1, 124.9, 79.8, 38.0, 32.0, 29.5, 29.4, 29.1, 23.9, 22.9, 21.6, 14.3; HRMS (ESI-TOF) calcd. for $C_{18}H_{28}O_2Na$ $[M+Na]^+$, 299.1987; found, 299.1979 $[M+Na]^+$.

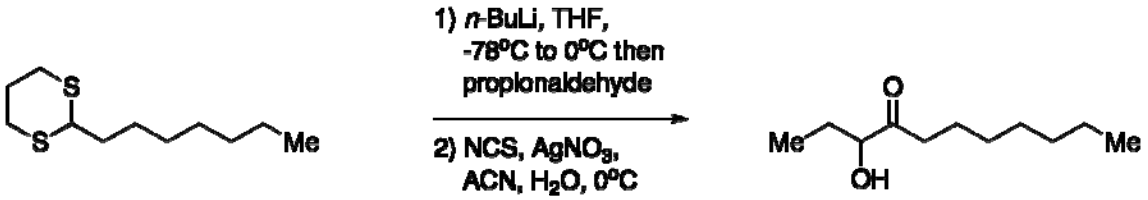

3-hydroxyundecan-4-one, C8-CAI-1. To a solution of 2-heptyl-1,3-dithiane (12) (1 g, 4.6 mmol) in THF (9.1 mL) at -78 °C was added *n*-butyl lithium (2.5 M in hexanes, 1.8 mL, 4.6 mmol) dropwise. The mixture was stirred with warming to 0 °C over 3 hours. After cooling to -78 °C, a solution of propionaldehyde (500 µL, 6.9 mmol) in THF (7 mL) was added dropwise. The reaction was allowed to slowly reach r.t. stirring overnight and was quenched with sat. NH_4Cl, extracted with 3 x 50 mL Et_2O, washed with brine and dried over Na_2SO_4, filtered, concentrated, and purified by silica gel chromatography (hexanes to 10%EtOAc/hexanes) to give 1-(2-heptyl-1,3-dithian-2-yl)propan-1-ol. Without further purification this product was dissolved in ACN (36 mL) at r.t. and H_2O (9 mL) was added followed by $AgNO_3$ (3.9 g, 22.9 mmol) and NCS (2.3 g, 20.5 mmol). The mixture was allowed to stir for 5 min and was quenched with sat. Na_2SO_3 (50mL), extracted with Et_2O, dried over Na_2SO_4, filtered, concentrated, and purified by silica gel chromatography (hexanes to 10%EtOAc/hexanes) to give 3-hydroxyundecan-4-one (517.2 mg, 61%, two steps). ^{1}H NMR (500 MHz, $CDCl_3$) δ 4.14 (dt, *J* = 6.7, 4.5 Hz, 1H), 3.51 (d, *J* = 4.9 Hz, 1H), 2.48-2.37 (m, 2H), 1.92-1.84 (m, 1H), 1.63-1.53 (m, 2H), 1.44-1.37 (m, 1H), 1.33-1.20 (m, 8H), 0.91 (t, *J* = 7.4 Hz, 3H), 0.85 (t, *J* = 7.0 Hz, 3H); ^{13}C NMR (125 MHz, $CDCl_3$) δ 212.7, 77.3, 38.0, 31.8, 29.4, 29.2, 26.9, 23.8, 22.8, 14.2, 9.1; HRMS (ESI-TOF) calcd. for $C_{11}H_{23}O_2$ $[M+H]^+$ 187.1698; found 187.1696 $[M+H]^+$

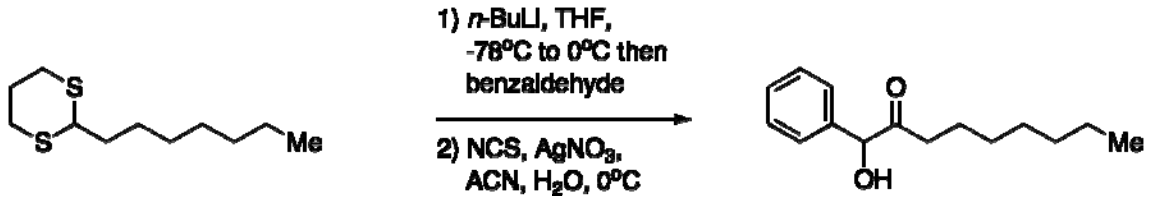

1-hydroxy-1-phenylnonan-2-one, C8-Phenyl-CAI1. To a solution of 2-heptyl-1,3-dithiane (12) (500 mg, 2.3 mmol) in THF (4.6 mL) at -78 ^{o}C was added *n*-butyl lithium (2.5 M in hexanes, 1.4 mL, 3.4 mmol) dropwise. The mixture was stirred with warming to 0 ^{o}C over 3 hours. After cooling to -78 ^{o}C, a solution of benzaldehyde (350 µL, 3.4 mmol) in THF (3.4 mL) was added dropwise. The reaction was allowed to slowly reach r.t. stirring overnight and was quenched with sat. NH_4Cl, extracted with 3 x 50 mL Et_2O, washed with brine and dried over Na_2SO_4, filtered, concentrated, and purified by silica gel chromatography (hexanes to 20%EtOAc/hexanes) to give (2-heptyl-1,3-dithian-2-yl)(phenyl)methanol. Without further purification this product was dissolved in ACN (46 mL) at -10 ^{o}C and H_2O (12 mL) was added followed by $AgNO_3$ (1.94 g, 11.4 mmol) and NCS (1.17 g, 10.3 mmol). The mixture was allowed to stir for 5 min and was quenched with sat. Na_2SO_3 (50mL), extracted with Et_2O, dried over Na_2SO_4, filtered, concentrated, and purified by silica gel chromatography (hexanes to 10%EtOAc/hexanes) to give 1-hydroxy-1-phenylnonan-2-one (305.4 mg, 57%, two steps).^{1}H NMR (500 MHz, $CDCl_3$) δ 7.38-7.26 (m, 5H), 5.05 (d, *J* = 4.4 Hz, 1H), 4.37 (d, *J* = 4.4Hz, 1H), 2.38-2.24 (m, 2H), 1.55-1.40 (m, 2H), 1.25-1.07 (m, 8H), 0.82 (t, *J* = 7.1Hz, 3H); ^{13}C NMR (125 MHz, $CDCl_3$) δ 209.9, 138.3, 129.2, 128.9, 127.6, 79.9, 38.0, 31.7, 29.1, 29.0, 23.9, 22.7, 14.3; HRMS (ESI-TOF) calcd. for $C_{15}H_{22}O_2Na$ $[M+Na]^+$, 257.1518; found, 257.1512 $[M+Na]^+$.

References:

1. Thelin KH & Taylor RK (1996) Toxin-coregulated pilus, but not mannose-sensitive hemagglutinin, is required for colonization by *Vibrio cholerae* O1 El Tor biotype and O139 strains. *Infect Immun* 64:2853-2856.

2. Ditta G, Stanfield S, Corbin D, & Helinski DR (1980) Broad host range DNA cloning system for gram-negative bacteria: construction of a gene bank of *Rhizobium meliloti*. *Proc Natl Acad Sci U S A* 77:7347-7351.
3. Sambrook J, Fritsch EF, & Maniatis T (1989) *Molecular Cloning: A Laboratory Manual* (Cold Spring Harbor Laboratory Press, Cold Spring Harbor, NY).
4. Simons RW, Houman F, & Kleckner N (1987) Improved single and multicopy lac-based cloning vectors for protein and operon fusions. *Gene* 53:85-96.
5. Bose JL, Rosenberg CS, & Stabb EV (2008) Effects of *luxCDABEG* induction in *Vibrio fischeri*: enhancement of symbiotic colonization and conditional attenuation of growth in culture. *Arch Microbiol* 190:169-183.
6. Svenningsen SL, Waters CM, & Bassler BL (2008) A negative feedback loop involving small RNAs accelerates *Vibrio cholerae*'s transition out of quorum-sensing mode. *Genes Dev* 22:226-238.
7. Swem LR, Swem DL, Wingreen NS, & Bassler BL (2008) Deducing receptor signaling parameters from in vivo analysis: LuxN/AI-1 quorum sensing in *Vibrio harveyi*. *Cell* 134:461-473.
8. Keymer JE, Endres RG, Skoge M, Meir Y, & Wingreen NS (2006) Chemosensing in *Escherichia coli*: two regimes of two-state receptors. *Proc Natl Acad Sci U S A* 103:1786-1791.
9. Higgins DA, *et al.* (2007) The major *Vibrio cholerae* autoinducer and its role in virulence factor production. *Nature* 450:883-886.
10. Johansson A, *et al.* (2003) Acyl sulfonamides as potent protease inhibitors of the hepatitis C virus full-Length NS3 (protease-helicase/NTPase): a comparative study of different C-terminals. . *Bioorganic & medicinal chemistry* 11:2551-2568.
11. Marshall JA & Belletire JL (1971) Heterolytic fragmentation of 1,3-dithianyl tosylates. *Tetrahedron Letters* 12:871-874.
12. Komatsu N, Uda M, & Suzuki H (1995) Bismuth(III) Halides and Sulfate as Highly Efficient Catalyst for the Sulfenylation of Carbonyl and Related Compounds. . *Synlett* 9 984-986.